Supplementary Fig. S1.

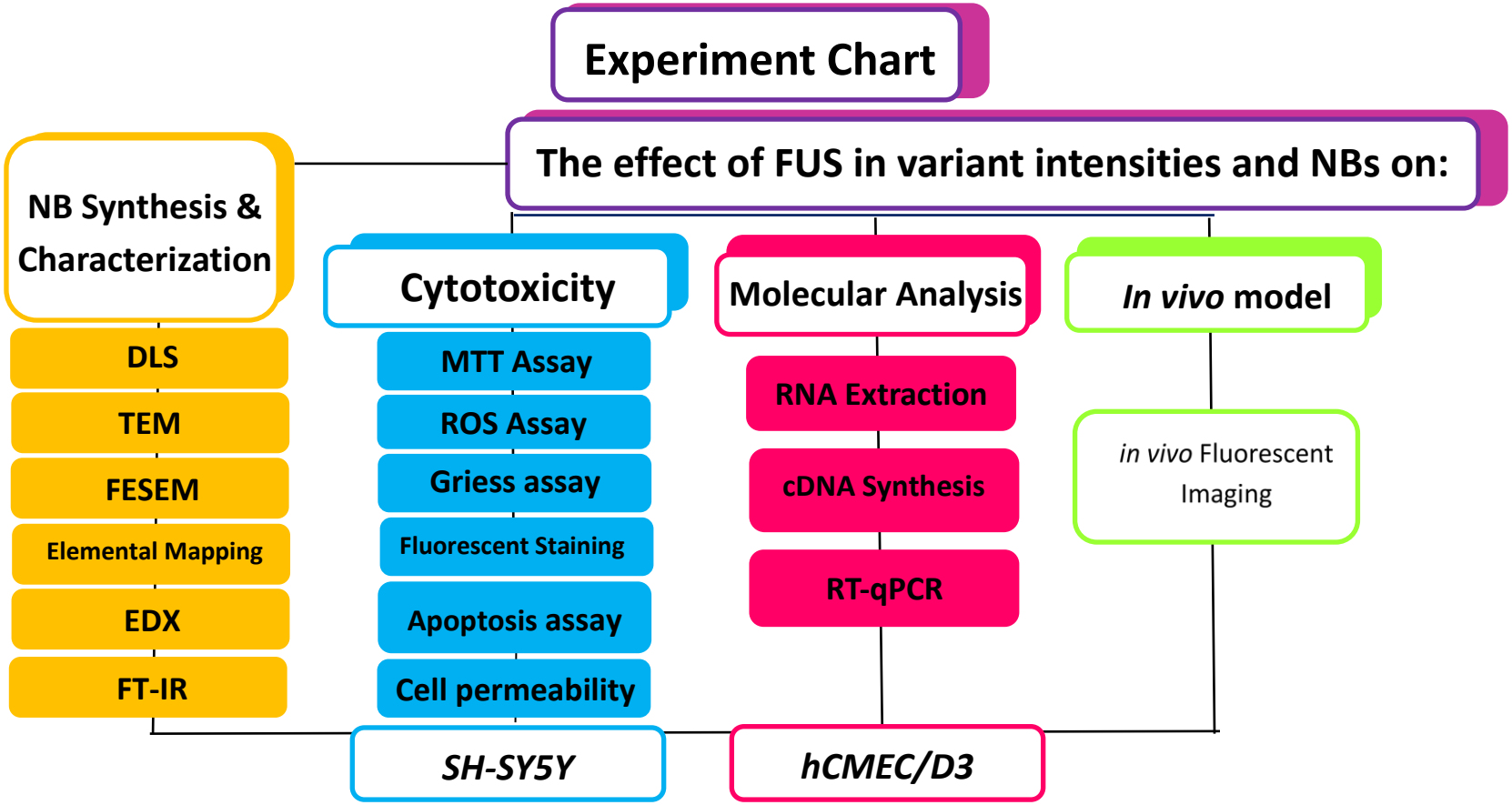

Fig. S1. ***Experiment chart.*** *The experiment assessing the effect of focused ultrasound intensities on drug delivery with nanobubbles was conducted in four stages: (1) synthesis of nanobubbles and drug loading, followed by characterization; (2) cell cytotoxicity studies; (3) molecular analyses; and (4) evaluation of drug targeted delivery through the blood-brain barrier in an animal model.*

Supplementary Fig. S2.

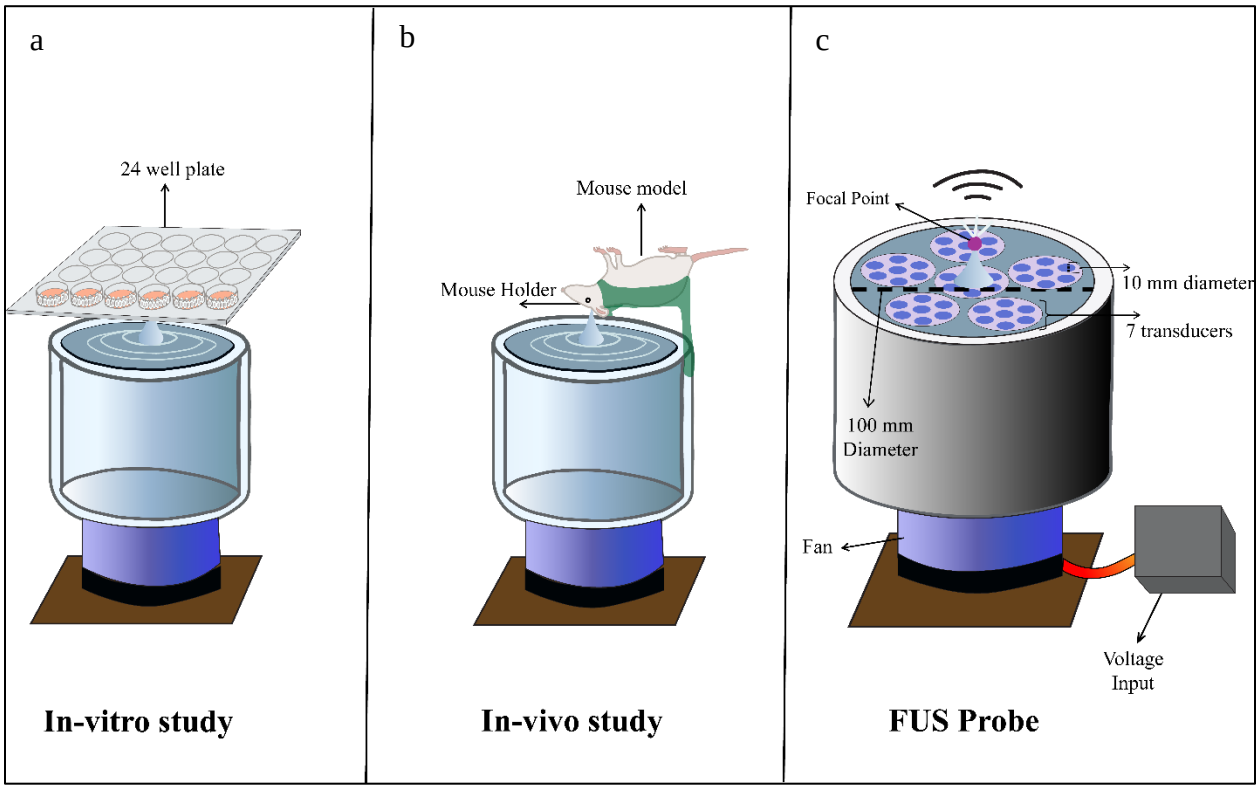

Fig. S2. ***Schematic illustration of the ultrasound exposure configurations used across the study.*** *(Left) In-vitro exposure setup: A custom 1.5-MHz hemispherical array was coupled to the culture plate via a degassed water bath to ensure uniform acoustic transmission. The 24-well plate was positioned at the geometric focus using alignment markers to maintain consistent focal placement across wells (Center) In-vivo mouse sonication setup: Anesthetized mice were placed on a custom holder above the coupling bath, enabling direct acoustic coupling through the skull. The focal point of the hemispherical array was aligned to a unilateral cortical hemisphere using stereotactic anatomical landmarks (bregma–lambda axis). (Right) Hemispherical array architecture: The FUS probe consists of seven 10-mm-diameter transducer modules arranged on a 100-mm-diameter hemispherical shell, producing a well-confined geometric focus. The diagram shows the relative element positioning, focal region, electrical input, and cooling fan used for thermal stabilization during prolonged sonications (created with Adobe Illustrator).*

Supplementary Fig. S3.

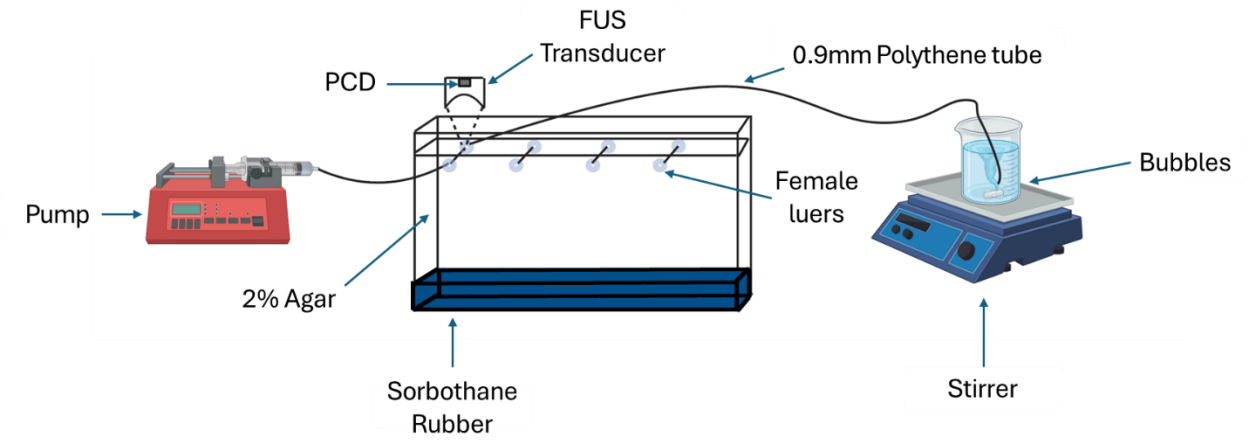

Fig. S3. ***Schematic representation of the experimental setup under FUS for*** **analysis of bubble cavitation.** *A 2% agar phantom was used, incorporating polyethylene tubing to simulate capillaries. FUS was delivered from the top via a single-element transducer with the focal point targeted on the capillary. The backscattered signals were captured with a PCD also positioned on the top. The setup included a syringe pump to withdraw nanobubbles from a beaker at a controlled rate (created with BioRender.com).*

Supplementary Fig. S4.

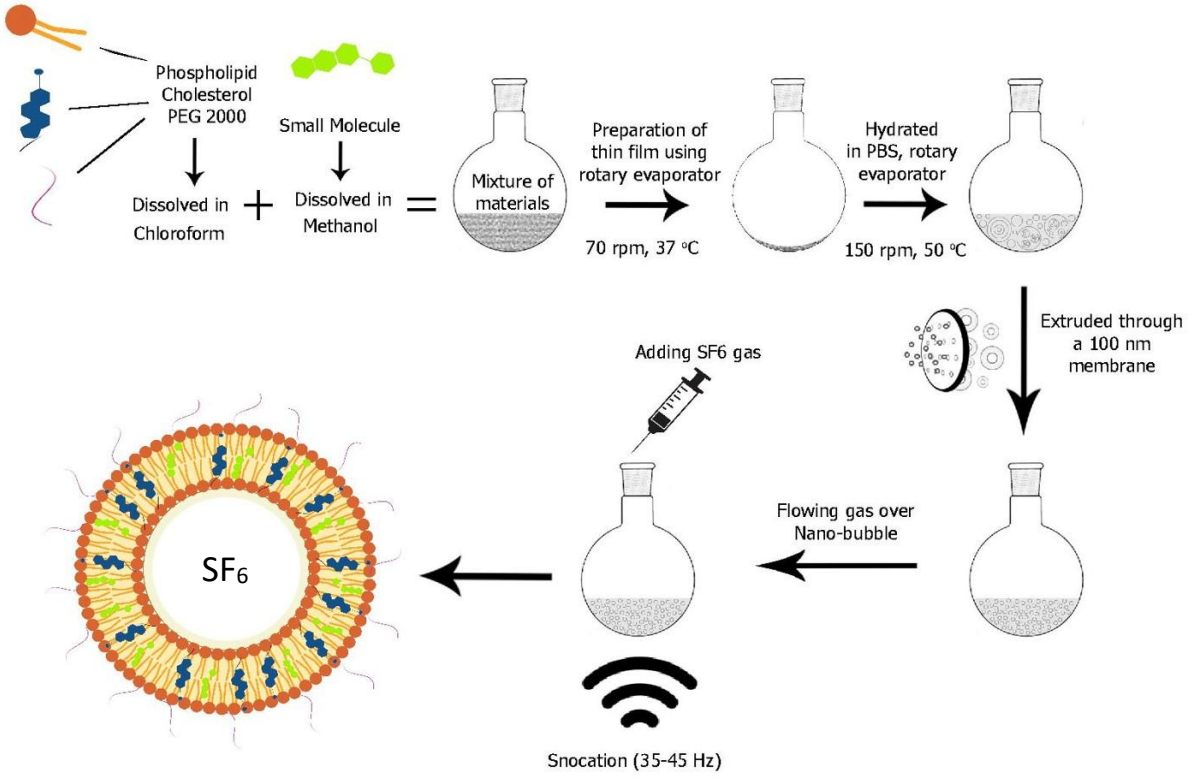

Fig. S4. ***Schematic diagrams illustrating the formation process of small molecule-loaded nanobubbles (SMOL-NBs) using SF6 gas.*** *Key steps depicted include: Thin-film formation, where the lipid or polymer film is created; Hydration, where the thin film is hydrated with an aqueous solution, leading to the swelling and dispersion of the film into multilamellar vesicles; Extrusion, where the resulting vesicles are passed through a nanofilter, producing uniformly sized nanobubbles encapsulating the small molecules and the final step of flowing SF6 gas over the nanobubbles to ensure gas encapsulation. (Created with (created with Adobe Illustrator).*

Supplementary Fig. S5.

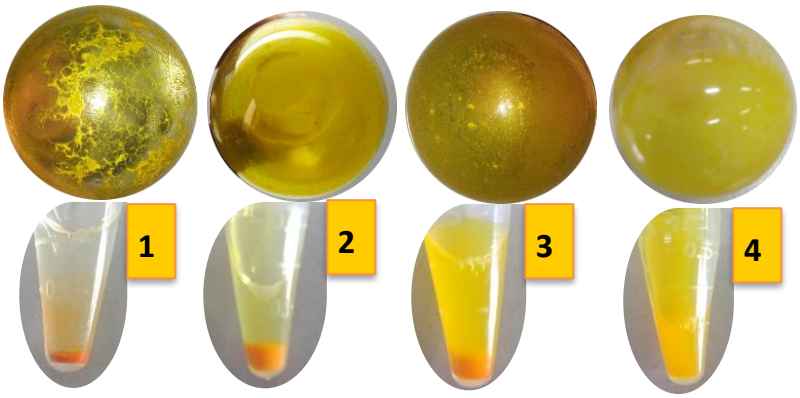

Fig. S5. ***Optimization of drug loading in nanobubbles***. *At higher curcumin-to-lipid ratio (1:3), insoluble curcumin particles were detected, suggesting that the 1:4 ratio is the optimal for effective drug encapsulation.*

Supplementary Fig. S6.

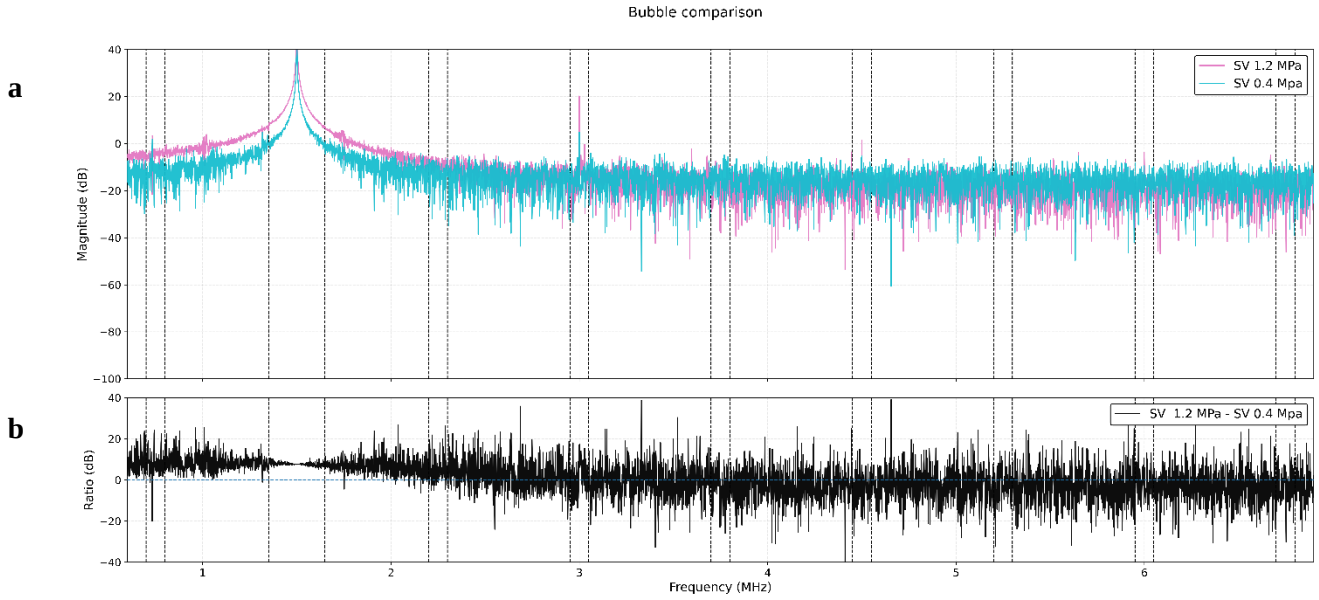

Fig. S6. Frequency-domain cavitation analysis of SV MBs at two acoustic pressures. (a) Representative FFT spectra of SV MBs at 0.4 MPa and 1.2 MPa. *FFT spectra of SV MBs acquired under 0.4 MPa and 1.2 MPa acoustic pressures. Harmonic, subharmonic, and ultraharmonic peaks are visible, accompanied by pronounced broadband noise at both pressures. The overall similarity of the spectra reflects the moderate effect size (Cohen's d) associated with SV MBs, indicating pressure-independent cavitation behavior and a consistent propensity for inertial cavitation even at lower pressures. (b)* ***Difference spectra for SV MBs at 0.4 MPa vs 1.2 MPa.*** *The difference spectrum obtained by subtracting the FFT at 0.4 MPa from that at 1.2 MPa shows broadband variations outside harmonic regions. Integration of this broadband region (AUC) followed by Wilcoxon statistical testing yielded $p < 0.001$, demonstrating measurable yet moderate pressure-dependent changes in inertial cavitation for SV MBs.*

Supplementary Fig. S7.

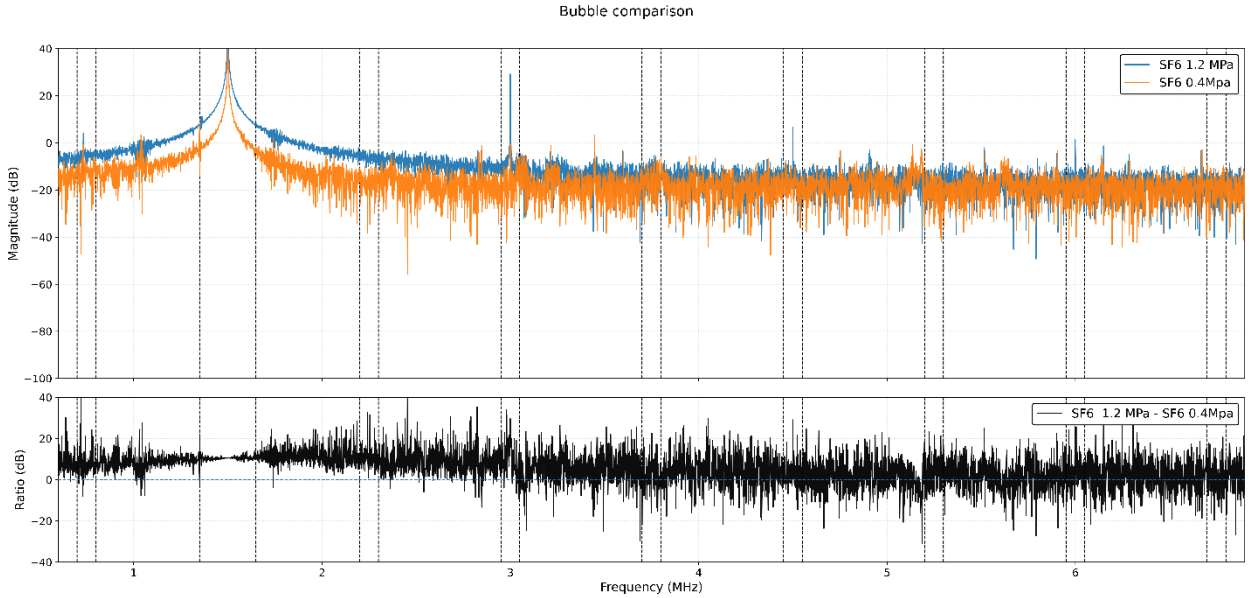

Fig. S7. Frequency-domain cavitation analysis of SF_6 NBs at two acoustic pressures. *(a) Representative FFT spectra of SF_6 nanobubbles at 0.4 MPa and 1.2 MPa. FFT spectra of SF_6 NBs showing damped, stable oscillations with minimal broadband noise at 0.4 MPa and enhanced harmonic activity at 1.2 MPa. Despite increased harmonic emission, inertial broadband noise remains comparatively low. The spectral differences across pressures are significantly larger than those of SV MBs, consistent with the very large effect size (Cohen's $d > 5$) calculated for SF_6.* ***(b) Difference spectra for SF_6 NBs at 0.4 MPa vs 1.2 MPa.*** *Difference spectra illustrate marked pressure-dependent modulation of broadband emissions for SF_6 NBs. AUC quantification of the broadband region (excluding harmonics) and Wilcoxon comparison yielded $p < 0.001$. The greater AUC differences relative to SV MBs confirm that SF_6 NBs exhibit stronger pressure-dependent spectral changes while maintaining low ICD levels overall.*

Supplementary Fig. S8.

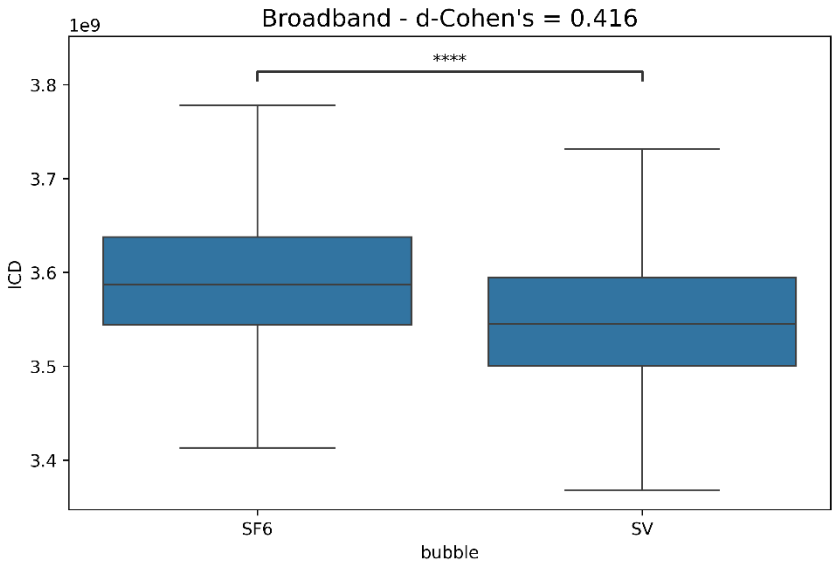

Fig. S8. Area Under the Curve of Spectral Differences Excluding Harmonics, Subharmonics, and Ultraharmonics. Bar plots showing the broadband AUC differences between 0.4 MPa and 1.2 MPa for each bubble type. Statistical analysis (Wilcoxon test, $p < 0.001$) demonstrates significantly larger spectral variation for SF_6 NBs. Effect size analysis indicates Cohen's $d = 0.42$ for the SF_6–SV comparison, reflecting a moderate positive effect and confirming that SF_6 NBs experience more pronounced pressure-dependent changes in inertial cavitation metrics than SV MBs. These results support the interpretation that SF_6 NBs maintain greater cavitation stability while exhibiting distinctive pressure-modulated behavior.

Supplementary Fig. S9.

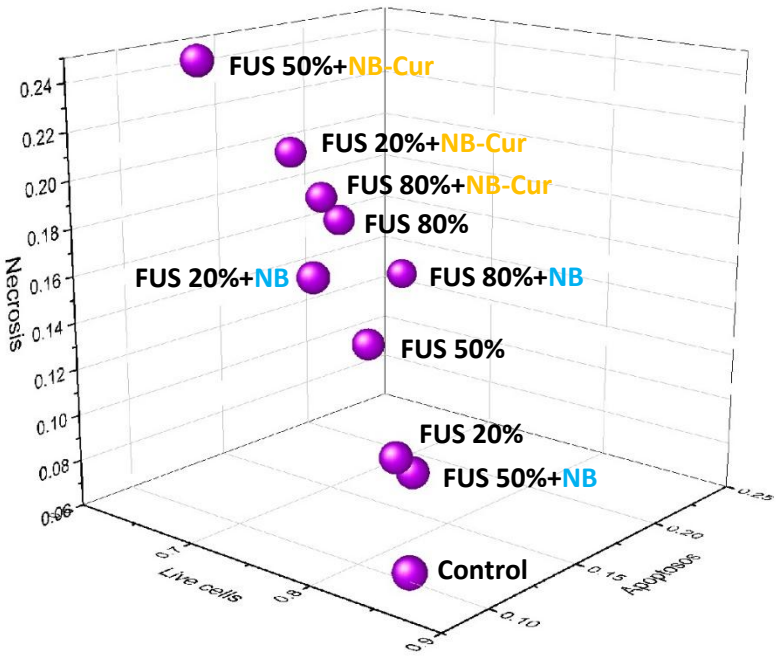

Fig. S9. *3D plot of Flow cytometry results to assess levels of viability, apoptosis and necrosis in SH-SY5Y cells under different experimental conditions.*

Supplementary Fig. S10.

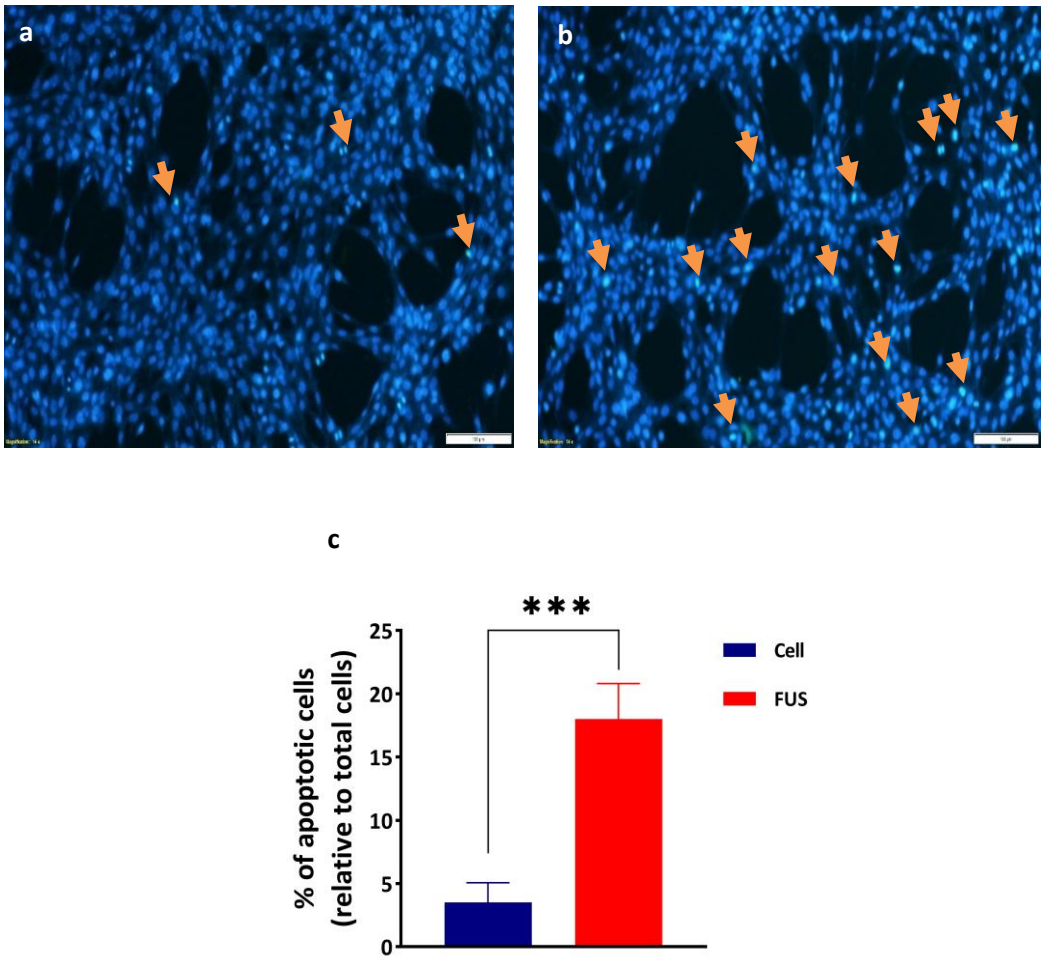

Fig. S10. Morphology of SH-SY5Y cells observed through DAPI staining. *Control cells (a) compared to FUS-treated cells after 6 hours (b) show an increase in cells with condensed and fragmented nuclei; Mean±SD, *** $P \leq 0.001$. Quantification of apoptotic cells, calculated using ImageJ software (c). Red arrows mark dead cells; scale bar: 100 µm.*

Supplementary Fig. S11.

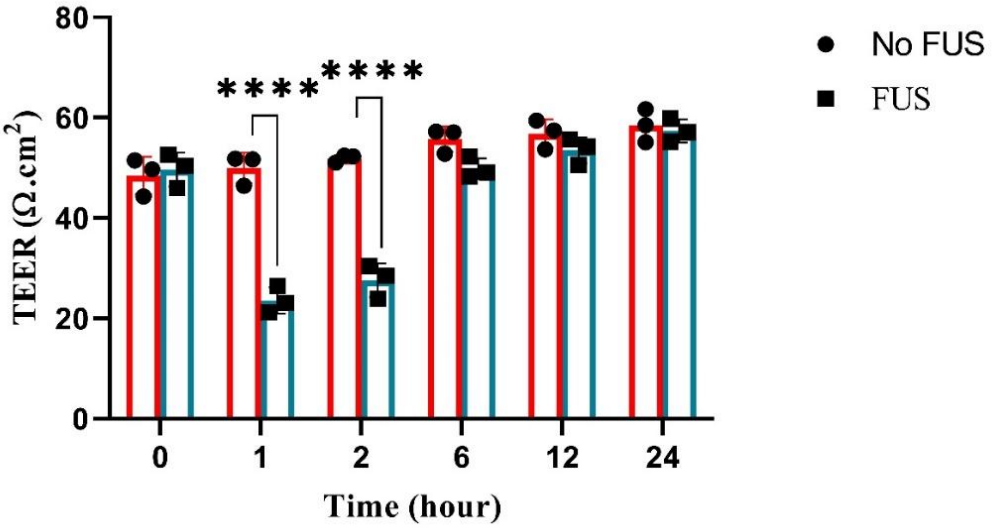

Fig. S11. ***Trans Endothelial Electrical Resistance (TEER) of hCMEC/D3 cells over time with and without FUS*** *The graph illustrates the changes in TEER (measured in ohms per square centimeter, Ω·cm²) over a 24-hour period. TEER values were recorded at 0, 1, 2, 6, 12, and 24 hours for cells treated with no FUS and 50% FUS. A significant decrease in TEER is observed in the FUS-treated group compared to the control group at multiple time points, indicating a potential disruption in the integrity of the cellular barrier. Statistical significance is indicated by asterisks (****p < 0.0001), showing a significant decrease in TEER in the FUS-treated groups.*

Supplementary Fig. S12.

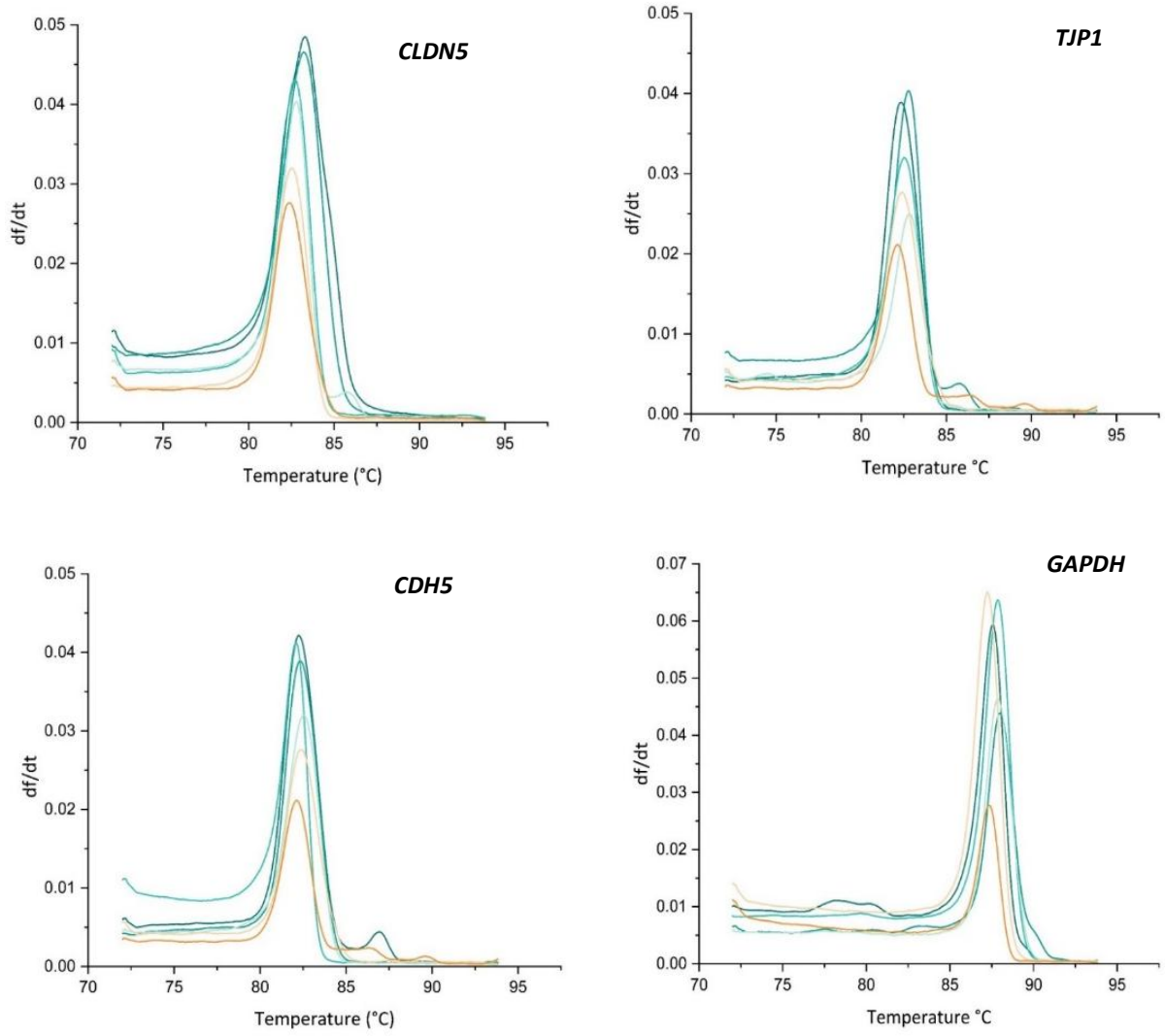

Fig. S12. ***Melting curve analysis of genes CLDN5, TJP1, CDH5, and GAPDH.*** *Melting curves for the genes CLDN5 (Claudin-5), TJP (Tight Junction Protein), CDH5 (Cadherin-5), and GAPDH (Glyceraldehyde 3-Phosphate Dehydrogenase). The distinct peaks indicate the specificity of the PCR products for each gene, confirming their amplification. GAPDH serves as the housekeeping gene for normalization.*

Supplementary Fig. S13.

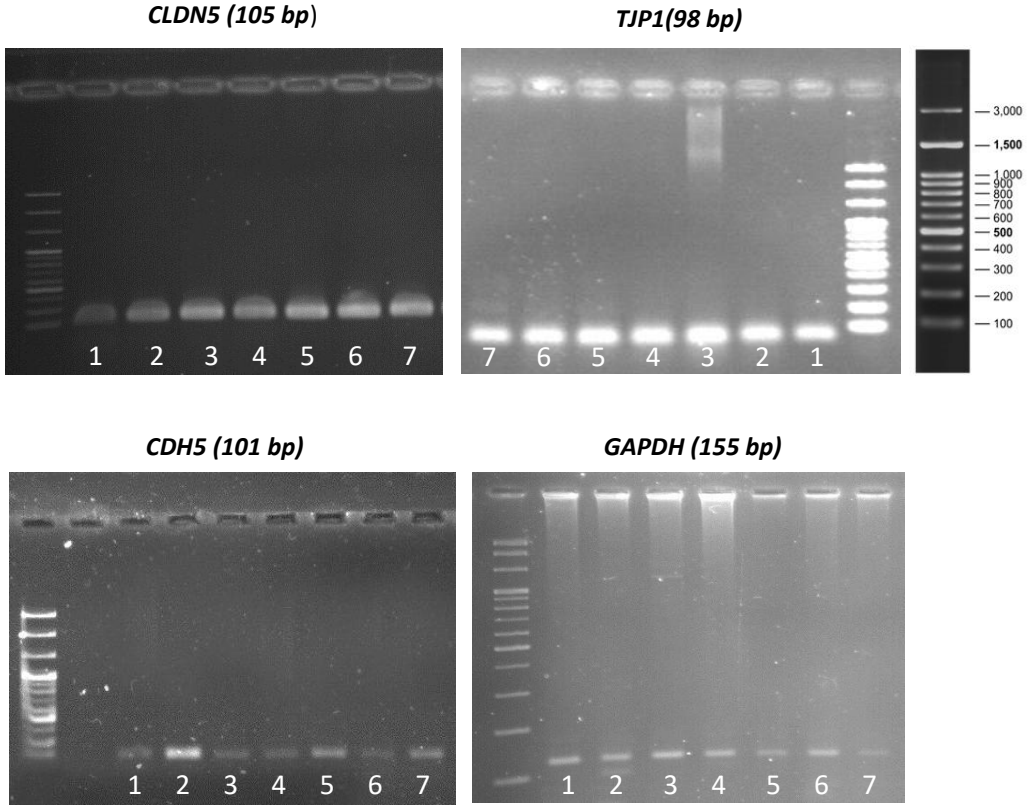

Fig. S13. ***Qualitative expression of CLDN5 (105 bp), TJP1 (98 bp), CDH5 (101 bp), and GAPDH (155 bp) genes in hCMEC/D3 by Real-Time PCR****. Lane1: Control, Lane 2: samples exposed 20% FUA, Lane 3: 20% FUS with nanobubbles containing Curcumin, Lane 4: 50% FUS, Lane 5: 50% FUS with nanobubbles containing Curcumin, Lane 6: 80% FUS, Lane 7: 80% FUS with nanobubbles containing Curcumin*

Supplementary Fig. S14.

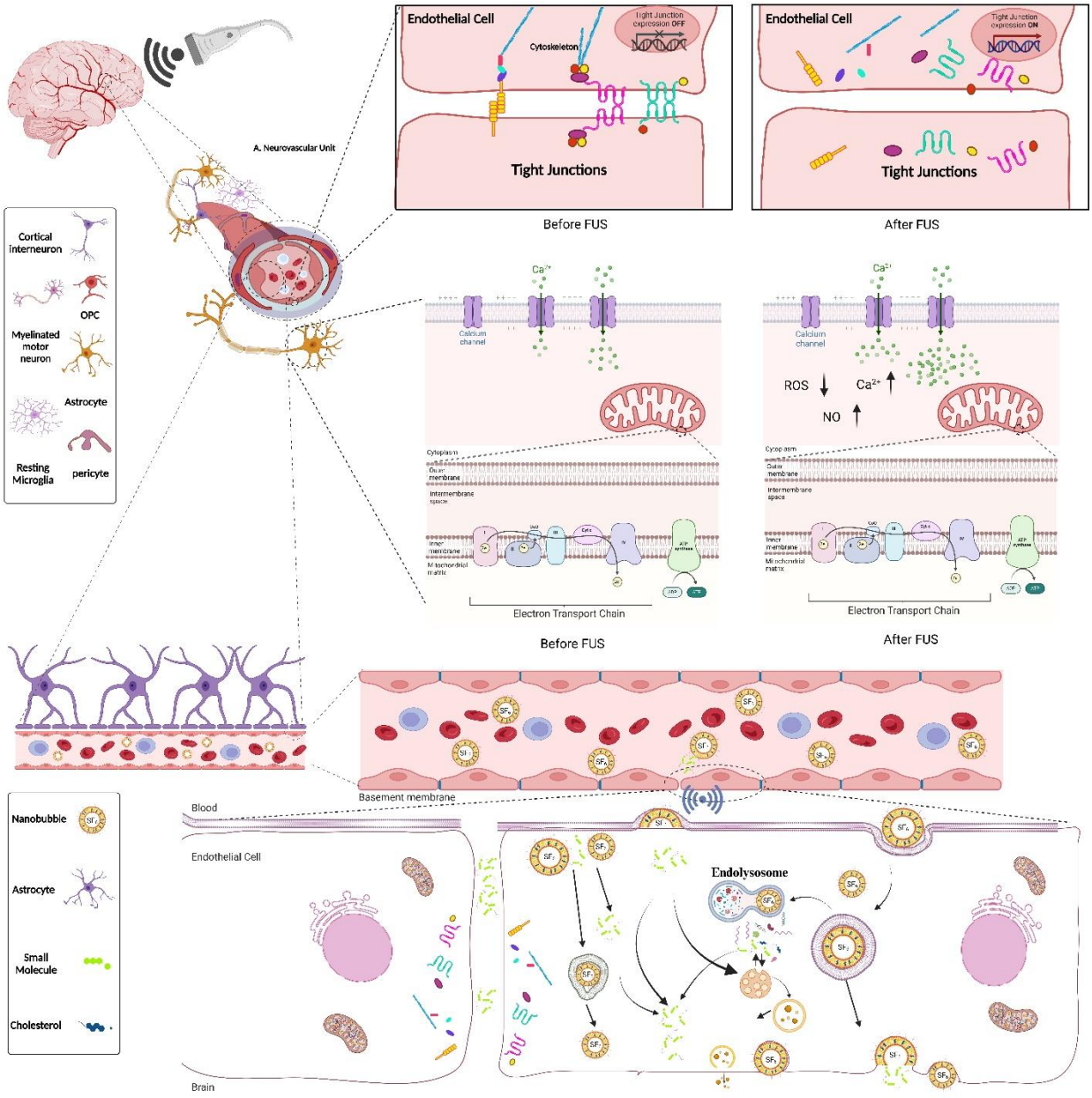

Fig. S14. Schematic representation of the mechanism and impact of small molecule-loaded NBs and FUS-mediated targeted delivery on the BBB and neuronal cells. *FUS, in combination with NBs, offers a non-invasive and reversible method to transiently permeabilize the BBB, enabling the targeted delivery of therapeutic agents. This approach ensures the safe delivery of drugs, as NBs remain structurally intact under FUS-induced pressure fluctuations across varying intensities. Importantly, low and high FUS intensities demonstrate no significant cytotoxicity in neuronal cells. FUS exerts mechanical effects on cells, facilitating the internalization of NB-Cur cargo through cell membrane poration. The pulsatile nature of FUS activates mechanosensitive ion channels, leading to calcium influx, membrane depolarization, and robust cellular responses that are critical for therapeutic effects. When applied at optimal intensities, FUS enhances the expression of BBB-related genes such as claudin-5, VE-cadherin, and ZO-1 in endothelial cells, supporting BBB integrity. Drug transport mechanisms facilitated by NBs include adsorption to the cell membrane, where membrane destabilization allows drug release and cellular uptake. Alternatively, NBs may be internalized via endocytosis, forming endosomes that either fuse with lysosomes for drug release or destabilize to deliver their cargo into the cytoplasm. Drugs can also be directly released into the cytoplasm through membrane fusion between NBs and the cell membrane. Illustration of the mechanism of drug delivery via NBs (created with BioRender.com)*

Supplementary Fig. S15.

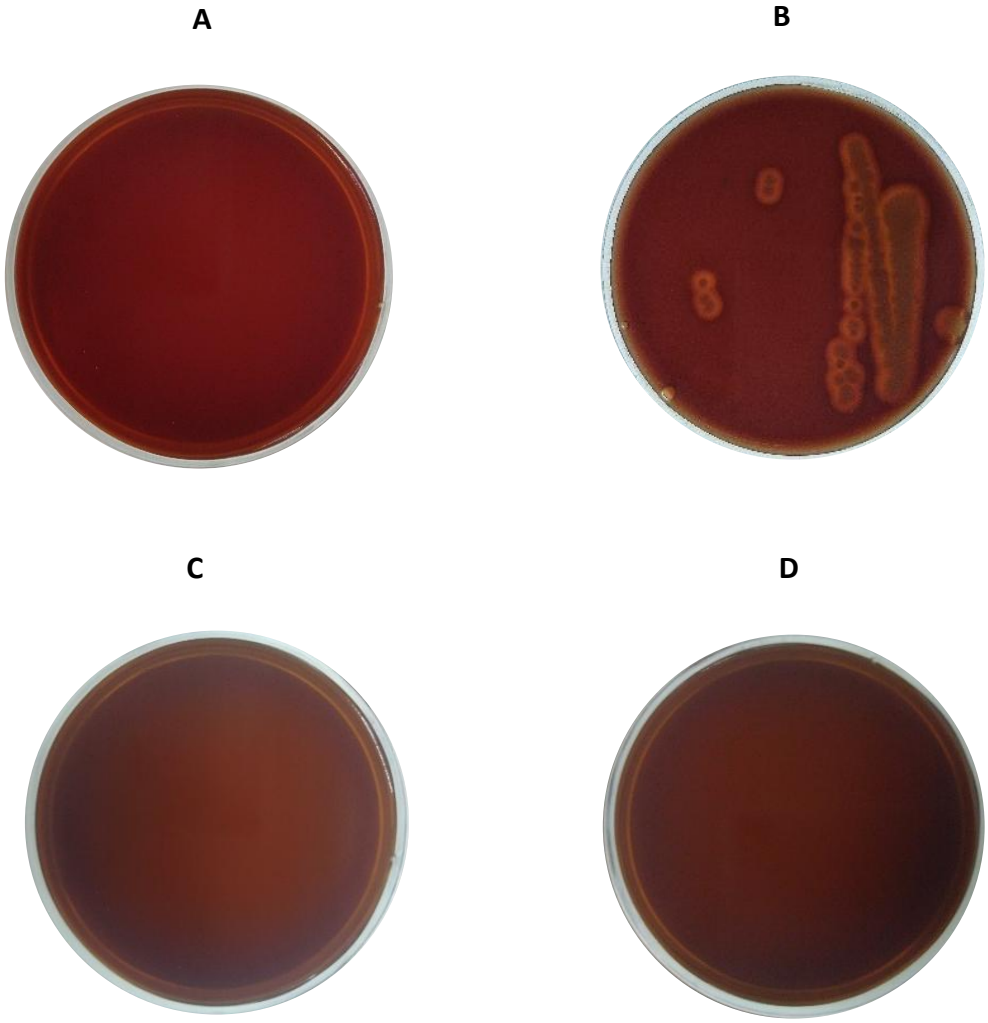

Fig. S15. Examining the hemocompatibility of the nanobubble containing curcumin. *A: No hemolysis with NB, B: Complete hemolysis in positive control (β-hemolysin) in the presence of Bacillus cereus, C: No hemolysis with Cur-NB, D: No hemolysis with FUS. 100 µL of NB, Cur-NB (final concentration of 100 µM based on the curcumin were applied onto a blood agar plate and incubated at 37 °C for 24 h. 100 µL of 0.5 McFarland of Bacillus Cereus was cultured under the same conditions. Absence of observable hemolysis was taken as an indicator of biocompatibility.*

Supplementary Fig. S16.

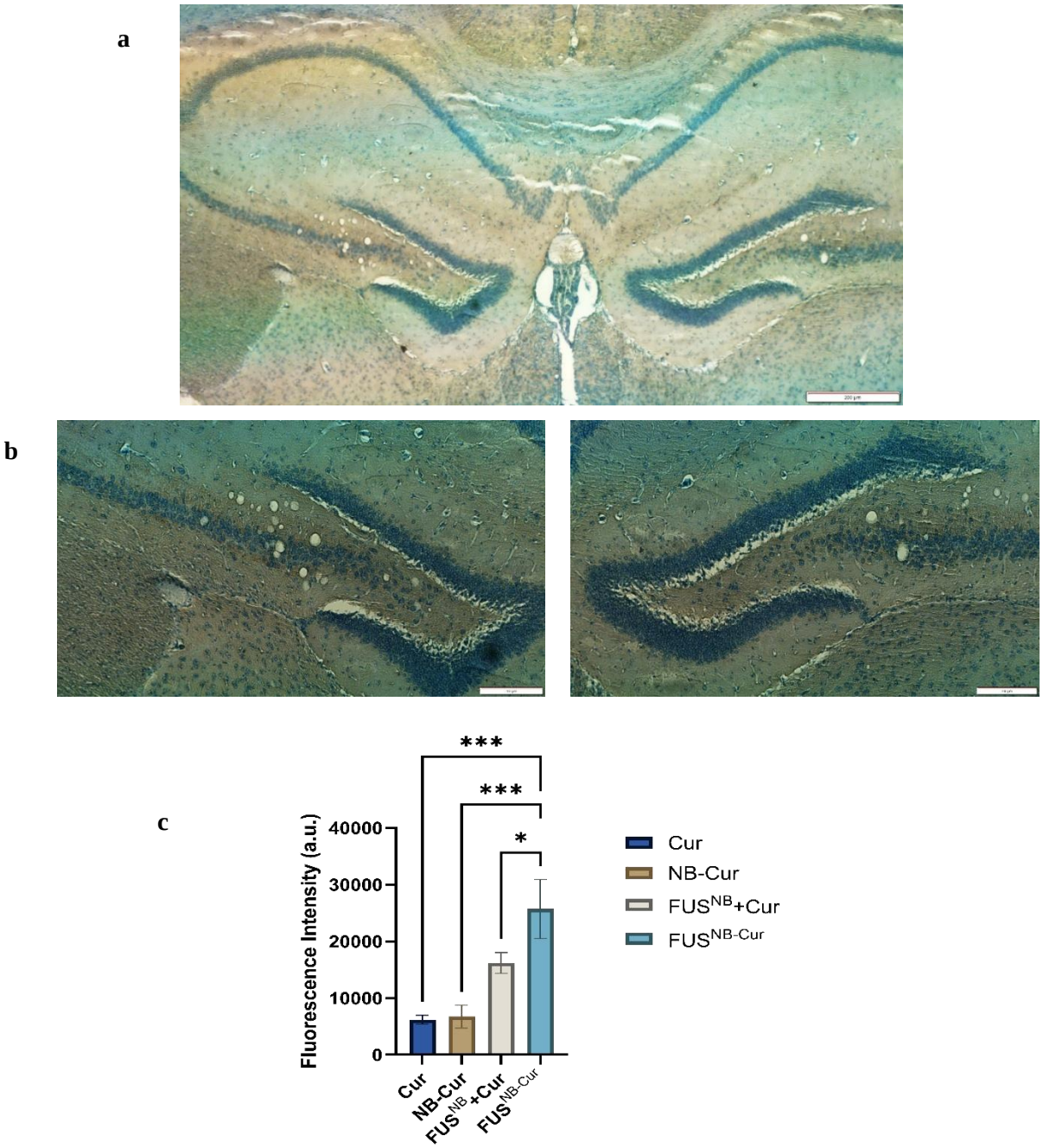

Fig. S16. Hematoxylin-eosin-stained horizontal brain sections of sonicated and control regions. *Top panel show low-magnification images of the brain section (a), while bottom panels show higher-magnification views of the sonicated and contralateral control regions (b). No gross tissue injury, hemorrhage, or neuronal damage was observed in either region, and overall cytoarchitecture remained intact, indicating the safety of the applied FUS parameters. Quantification of brain fluorescence intensity following systemic administration of curcumin in different formulations (c) (mean ± SD, n=3).*

Supplementary Table. S1, Table. S2, Table. S3.

Table S1. Comparative Specifications of the Hemispherical Array and the Single-Element Transducer

Parameter	Hemispherical Array (42-element)	Single-Element Transducer
Transducer type	42-element hemispherical phased array	Spherically focused single element
Operating frequency	1.5 MHz	1.5 MHz
Element / aperture diameter	10 mm per element; 102 mm outer aperture	25 mm aperture
Geometric focal length	50 mm (hemispherical shell radius)	20 mm (radius of curvature)
f-number	≈ 0.5	≈ 0.8
Axial FWHM	≈ 3 mm	≈ 2 mm
Lateral FWHM	≈ 0.6 mm	≈ 0.8 mm
Application	In vitro sonication; in vivo mouse brain exposures	Benchtop acoustic characterization only

Table S2. Normalized Intensity Relative to FUS parameters of Hemispherical Array Device.

Number	Normalized Intensity (%)	ISPTA (W/cm^2, DC 10%)	ISPPA (W/cm^2)	peak negative pressure (MPa)	mechanical index
I	20	0.133	1.33	0.2	0.1
II	50	0.533	5.33	0.4	0.3
III	80	4.8	48	1.2	0.9

Table S3. Drug and Lipid Concentration Ratios.

No.	Drug Concentration	Lipid Concentration	Drug: Lipid portion
1	4 mM	12 mM	1:3
2	3 mM	12 mM	1:4
3	2.4 mM	12 mM	1:5
4	2 mM	12 mM	1:6

Supplementary Table. S4.

Table S4. The characteristics of curcumin and nanobubble compounds extracted from PubChem

Chemical compound name	Molecular Weight (g/mol)	XLogP3	Hydrogen Bond Donor Count	Hydrogen Bond Acceptor Count	Chemical structure
Curcumin	368	3.2	2	6	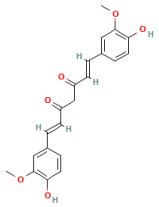
DPPC	734	13	0	8	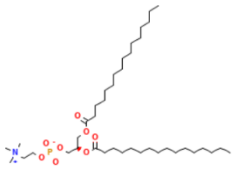
Cholesterol	386	8.7	1	1	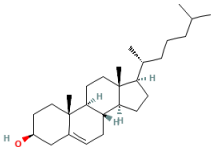
DSPE-PEG-Maleimide (MW 2000)	1076	-	3	14	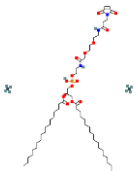

Supplementary Table. S5, Table. S6, Table. S7, Table. S8.

Table S5. The hydrodynamic diameters, zeta potentials, DEE% and DLC% of cucumin-loaded nanobubbles. The data represent mean values for n=3.

	Particle size	PDI	Zeta potential (mV)	DEE (%)	DLC (%)
NB-Cur	109	0.161	-1.53	88 ±2.98	3 ±0.56

Table S6. energy-dispersive X-ray spectroscopy (EDS) Elemental analysis of NB-Cur.

Element	Line Type	Apparent Concentration	k Ratio	Wt%	Wt% Sigma	Atomic %	Standard Label	Factory Standard
C	K series	0.19	0.00194	47.56	1.96	55.09	C Vit	Yes
N	K series	0.00	0.00000	0.00	0.00	0.00	BN	Yes
O	K series	0.31	0.00105	47.44	1.97	41.25	SiO2	Yes
F	K series	0.03	0.00007	5.00	2.85	3.66	CaF2	Yes
P	K series	0.00	0.00000	0.00	0.00	0.00	GaP	Yes
S	K series	0.00	0.00000	0.00	0.00	0.00	FeS2	Yes
Total				100.00		100.00		

Table S7. characteristic common peaks of FTIR for the nano bi-layer and NB-Cur spectrum.

Absorption (cm^{-1})	Functional Group	IR Spectrum Range (cm^{-1})	Compound Class	NB-Cur component
1424	O-H stretching	1420-1330	alcohol	Cholesterol
1489	N-O stretching	1550-1480	nitro compound	DPPC & DSPE-PEG 2000
2985	N-H stretching	3000-2800	amine	DSPE-PEG 2000
2826	O-H stretching	3200-2700	alcohol	Cholesterol
2890	C-H stretching	3000-2840	alkane	DPPC & DSPE-PEG 2000 & cholesterol

Table S8. characteristic exclusive peaks of FTIR for NB-Cur spectrum.

Absorption (cm^{-1})	Functional Group	IR Spectrum Range (cm^{-1})	Compound Class	NB-Cur component
3440	O-H stretching	3550-3200	alcohol	Curcumin
1636	C=C stretching	1662-1626	alkene	Curcumin
1354	S-O stretching	1370-1335	sulfonamide	SF6
1095	C-F stretching	1400-1000	Fluoro compound	SF6

Supplementary Table. S9.

Table S9. Comparison of ICD and SCD fold-changes across SF6 NBs/SV MBs types and acoustic pressures.

Comparison	Fold Change ICD	Fold Change SCD
SF_6 vs SV at 0.4	-3.468	-4.953
SF_6 vs SV at 1.2	0.007	0.949
SF_6 at 0.4 - SF_6 at 1.2	-5.218	-5.287
SV at 0.4 - SV at 1.2	-3.581	-2.118

Supplementary Table. S10, Table. S11.

Table S10. Primers sequences used for measuring the expression level of BBB specific genes.

Gene name	5′-3′ Prime Sequence	melting point	Amplicon length (bp)
CLDN5	CTGGACCACAACATCGTGAC CACCGAGTCGTACACTTTGC	58/85 59/22	105
CDH5	GCATAGCATTGGATACTCCATC CTCTGTCCAGTTCTTTCTCATTG	56/78 57/14	101
TJP1	TTCTCTTCCAGAACCAAAGCCT GAGTTGAATTAGGTAGGACACC	59/56 55/91	98
GAPDH	CTCATGACCACAGTCCATGC TTCAGCTCTGGGATGACCT	58/62 57/59	155

Table S11. **Effect of FUS at different intensities on the cell viability.** The percentages of live cells, early apoptosis, late apoptosis, and necrosis were determined using flow cytometry analysis.

	***SH-SY5Y* cells**	**Live Cells**	**Early Apoptosis**	**Late Apoptosis**	**Necrosis**
a	Control	83.4%±1.25	4.55%±1.19	5.92%±0.45	6.08%±0.64
b	FUS 20%	77.3%±0.13	6.96%±1.28	6.94%±0.3	8.82%±1.05
c	FUS 20%+NB	70.4%±1.02	5.66%±0.18	8.22%+0.047	15.7%±0.28
d	FUS 20%+NB-Cur	62.8%±0.064	4.34%±0.42	13.1%±0.37	19.7%±1.02
e	FUS 50%	71.4%±0.034	7.97%±1.32	8.33%±0.73	12.3%±0.063
f	FUS 50%+NB	77.3%±1.82	8.47%±0.09	6.40%±1.09	7.86%±0.66
g	FUS 50%+NB-Cur	63.3%±0.29	3.33%±0.049	8.87%±2.06	24.5%±0.46
h	FUS 80%	64.2%±0.12	10.8%±0.17	8.55%±1.57	16.4%±0.55
i	FUS 80%+NB	63.4%±0.46	10.2%±0.23	13.6%±0.38	12.8%±0.097
j	FUS 80%+NB-Cur	64.0%±0.037	8.90%±1.02	9.53%±0.86	17.6%±0.03

Supplementary Table. S12, Table. S13.

Table S12. Defined parameters for heat transfer equations.

Parameter	Density (kg/m^3)	Speed of Sound (m/s)	Thermal Conductivity (W/m·K)	Heat Capacity (J/kg·K)
Water	1000	1483	0.6	**4200**
Polypropylene	905	2200	0.22	**1800**

Table S13. Defined values for the boundary between the wall and water, and the boundary between water and air.

Convective Heat Transfer Coefficient with Air ($W/K \cdot m^2$)	Attenuation Coefficient for Ultrasound Waves (Np/m)
20	**0.22**
10	**10**